J. metamorphic Geol., 2009, **27,** 621–638 doi:10.1111/j.1525-1314.2009.00848.x

The Luliangshan garnet peridotite massif of the North Qaidam UHPM belt, NW China – a review of its origin and metamorphic evolution

S. G. SONG,[1] Y. L. NIU,[2] L. F. ZHANG[1] AND K. BUCHER[3]
[1]*MOE Key Laboratory of Orogenic Belts and Crustal Evolution, School of Earth and Space Sciences, Peking University, Beijing 100871, China (sgsong@pku.edu.cn)*
[2]*Department of Earth Sciences, Durham University, DH1 3LE Durham, UK*
[3]*Institute of Mineralogy and Geochemistry, University of Freiburg, Albertstrasse 23b, D-79104 Freiburg, Germany*

ABSTRACT The Luliangshan garnet peridotite massif is an ultramafic complex in the North Qaidam UHPM belt, NW China. The strongly layered complex comprising garnet-bearing dunite, garnet-harzburgite, garnet-lherzolite and garnet-pyroxenite and garnet-free dunite, occurs together with eclogite embedded in various continental gneisses. The geological setting, the internal structure, bulk-composition, rare earth elements, isotopic and mineral composition data show that the garnet peridotite derives from a middle Ordovician Alaskan-type layered sub-arc cumulate intrusion of ascending mantle wedge melts. An abyssal peridotite protolith can be excluded. During the Ordovician-Silurian continental collision, thickening and foundering, the Luliangshan peridotite complex was exposed to ultrahigh pressures (UHP) reaching 5.5 GPa possibly >6 GPa at temperatures of 900 °C (perhaps up to 1000 °C) corresponding to a depth of $\sim$200 km. The extreme pressure conditions have been derived from thermobarometry using mineral compositions of the garnet peridotite assemblages, but they are supported by a wealth of decompression-induced mineral exsolutions in UHP minerals and by diamond inclusion in zircon. The Luliangshan garnet peridotite has experienced four stages of retrograde overprint during exhumation that lasted into the Devonian: (i) decompression-induced unmixing of the UHP minerals; (ii) garnet kelyphitisation; (iii) amphibole overprinting and (iv) serpentinization. Hydrous minerals occurring within peak metamorphic assemblage represent pseudo-inclusions, that is reaction products of reactions related to various stages of decompression and cooling rather than prograde inclusions during porphyroblast growth.

Key words: Alaskan-type ultramafic cumulates; continental subduction and exhumation; garnet peridotite; metamorphic evolution; North Qaidam.

INTRODUCTION

Garnet peridotites occuring together with eclogite in gneisses of the continental crust in orogenic belts are characteristic of continental-type deep subduction. They are widespread within ultrahigh-pressure metamorphic (UHPM) belts resulting from continental collision (Medaris & Carswell, 1990), thickening and foundering of continental material. This geodynamic setting and their ultra-deep origin (>6 GPa) in some UHP terranes (Yang *et al*., 1993; Dobrzhinetskaya *et al*., 1996; Green *et al*., 1997; Bozhilov *et al*., 1999; van Roermund & Drury 1998; van Roermund *et al*., 2000, 2002; Song *et al*., 2004, 2005a,b; Zhang *et al*., 2000; Spengler *et al*., 2006) makes garnet peridotites an important window to the geodynamic processes of continental subduction, collision, exhumation and crustal–mantle interaction on a regional scale with global geodynamic implications.

The Luliangshan garnet peridotite massif is a large ultramafic body in the North Qaidam UHPM belt, a 400-km-long continental collision belt of the Early Palaeozoic at the northern edge of the Tibetan Plateau. It was first reported by Yang *et al*. (1994) and further studied by Song *et al*. (2004, 2005a,b, 2007) and Yang & Powell (2008). Mineral exsolution lamellae of rutile + two pyroxene + sodic amphibole in garnet and ilmenite + Al-chromite in olivine (Song *et al*., 2004, 2005a) as well as the presence of a diamond inclusion in a zircon, suggest that this peridotite body experienced ultraUHPM at depths in excess of 200 km.

New data are presented for the Luliangshan garnet peridotite that further support ultra-deep subduction of the peridotite and suggest a complex protolith assemblage including sub-arc continental lithospheric harzburgite and primitive arc melt cumulate, rather than serpentinized abyssal peridotite (Yang & Powell, 2008).

GEOLOGICAL SETTING

The North Qaidam UHP metamorphic belt is a distinctive continental subduction and exhumation orogenic belt of Palaeozoic age in Northwest China. It extends from Dulan northwestward to Yuka for ~400 km, and it is offset for up to 400 km by the Altyn Tagh Fault, a large NE-striking sinistral strike-slip fault (Fig. 1). The fault cuts through blocks of late Precambrian crystalline basement of similar age (e.g. Wan *et al*., 2001; Song *et al*., 2006). Further to the north is the Qilian terrane with an Early Palaeozoic oceanic-type suture (i.e. see Song *et al*., 2006, 2009a and references therein). The Qaidam block is located south of Precambrian basement units. It represents a Mesozoic intercontinental basin underlain by a Precambrian basement (e.g. Song *et al*., 2006).

The North Qaidam UHP belt mainly consists of a typical continental-type subduction-zone setting. Coesite and diamond inclusions in zircon and garnet suggest UHP conditions that are similar to other continental-type UHPM terranes elsewhere in the world (Yang *et al*., 2001, 2002; Song *et al*., 2003a, 2005b). Zircon SHRIMP dating reveals that the HP and UHP metamorphic ages of the North Qaidam UHP belt range from 460 to 400 Ma (Song *et al*., 2003b, 2005a, 2006; Mattinson *et al*., 2006, 2009; Zhang *et al*., 2008a,b; Chen *et al*., 2009). Consequently, parts of the Precambrian basement of the Qaidam block have been subducted and metamorphosed in the Upper Ordovician to Lower Devonian period.

Within this Palaeozoic orogenic belt two distinct types of peridotites can be distinguished: (i) the Luliangshan peridotite complex (Figs 1 & 2) consists of garnet peridotite derived from ultramafic cumulates from a continental arc and (ii) the Shaliuhe serpentinized harzburgite from UHP metamorphosed early Palaeozoic ophiolite sequences in the Dulan Terrane (Song *et al*., 2007, 2009b; Zhang *et al*., 2008a).

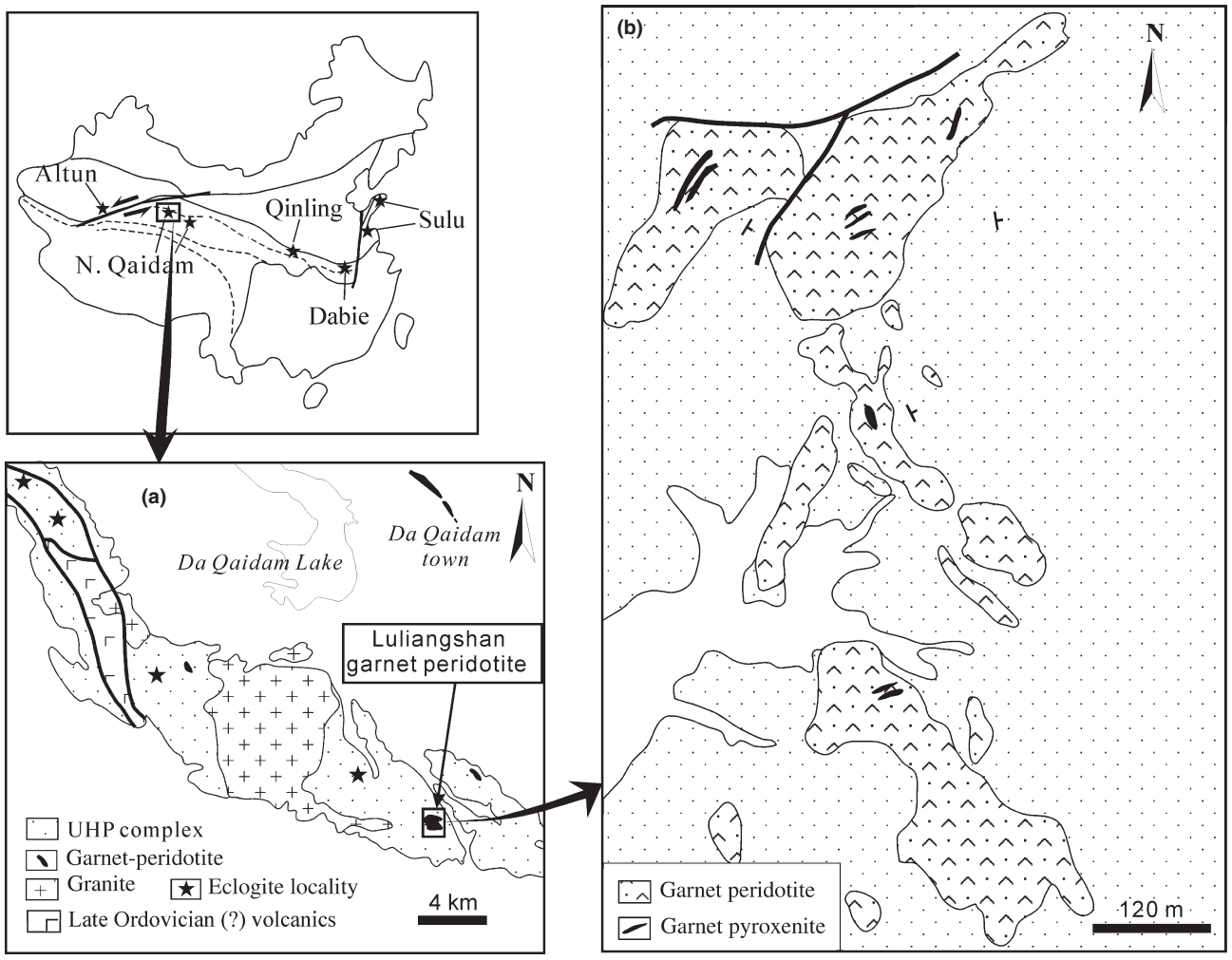

Fig. 1. (a) Geological overview and location map of the Luliangshan garnet peridotite body. (b) Geological map of the garnet peridotite (after Song *et al*., 2004).

PETROGRAPHY, WHOLE-ROCK AND MINERAL COMPOSITIONS

The Luliangshan garnet peridotite forms a large massif body ~500–800 m in size within an eclogite-bearing quartzofeldspathic gneiss terrane of the North Qaidam UHPM belt. The peridotite is a layered ultramafic complex in which four rock types have been recognized (Song *et al*., 2005b, 2007): (i) garnet-free dunite; (ii) garnet-bearing dunite and harzburgite; (iii) garnet lherzolite and (iv) garnet pyroxenite.

Coarse-grained dunite comprises strongly serpentinized olivine (>95 vol%) with minor orthopyroxene (Opx) and Cr-rich spinel (Spl). It occurs as up to 10 m thick brown-coloured bands within black-coloured garnet lherzolite and garnet-bearing dunite (Fig. 2a,b). Locally thin dunite bands alternate with garnet dunite and garnet lherzolite layers (Fig. 2c) on the scale of some centimetres. The fine banded structure resembles that of Alaskan-type ultramafic cumulates (Himmelberg & Loney, 1995; Scheel *et al*., 2005).

Garnet-bearing dunite and garnet harzburgite with a coarse-grained equigranular texture contains ~90% olivine ($Fo_{0.906–0.920}$) and variable amounts of garnet (Grt), Opx and clinopyroxene (Cpx). The rocks form layers varying in thickness from 10 cm to 2 m within garnet lherzolite or as rhythmic bands that gradually change from garnet-bearing dunite to harzburgite to garnet lherzolite (Fig. 2c). Garnet is porphyroblastic and Mg-rich with 69–75 mol% pyrope, 11–18% almandine, 3–8% grossular, 0.8–2.0% spessartine and 3–6% uvarovite. Fine-grained Cr-spinel occurs as a product of decompression-induced breakdown of earlier high-Cr garnet and pyroxene.

Garnet lherzolite clearly dominates with ~70–80 vol.% the peridotite massif. The different peridotites occur as band and layers of varying thickness (centimetres–metres) and the bands usually show sharp lithological boundaries. Garnet lherzolite bands or olivine-websterite bands are present depending on pyroxene abundances at various scales. garnet-dunite or garnet-harzburgite and garnet-lherzolite display

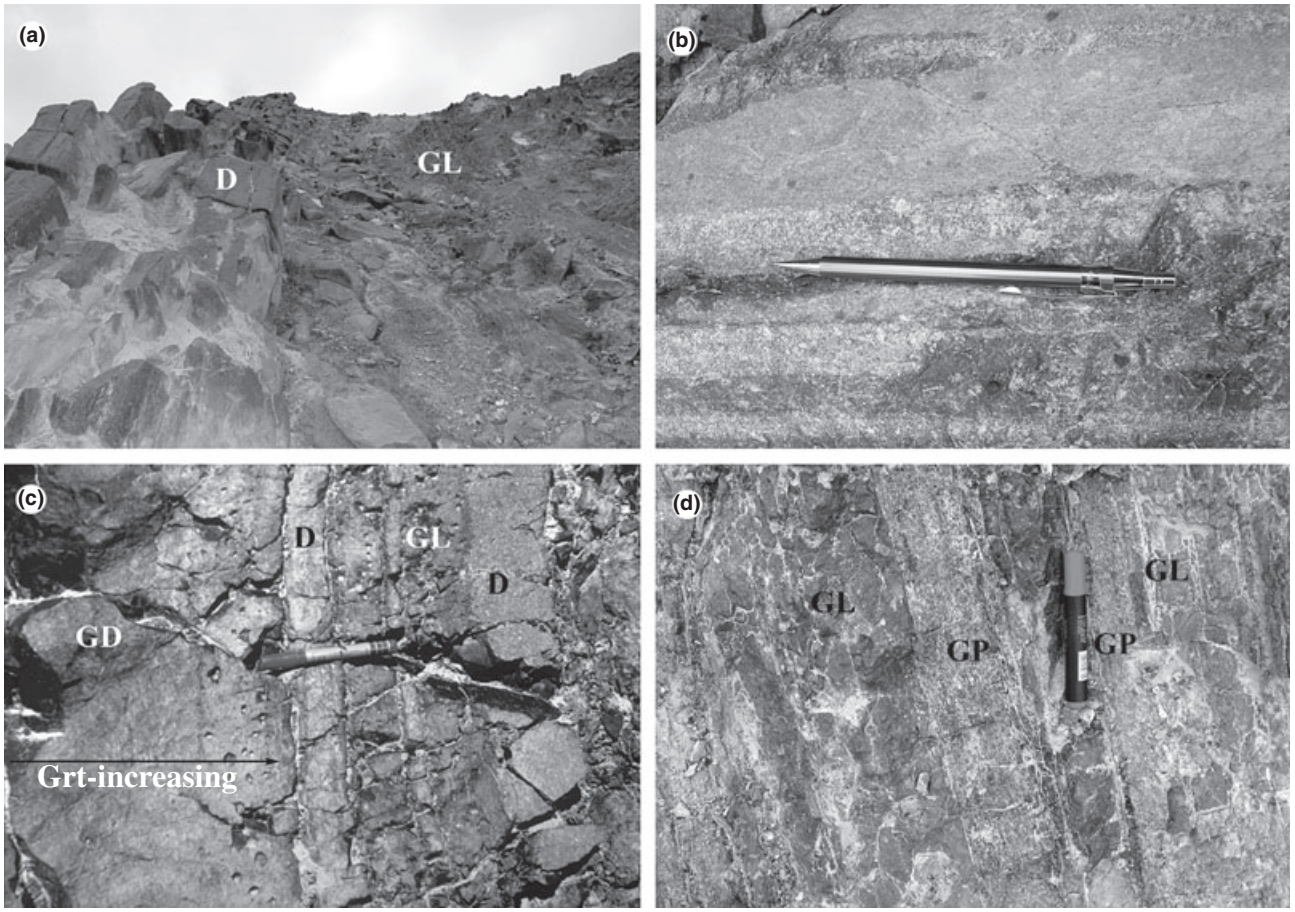

Fig. 2. Photographs showing field occurrences of various rock types of the Luliangshan garnet peridotite massif. (a) Massive garnet-free dunite (d) interlayered with garnet lherzolite (GL); (b) banded structure of dunite; (c) rhythmic variation of garnet content in garnet peridotite from harzburgite to lherzolite, garnet-free dunite occurs as interlayers; (d) garnet lherzolite interlayered with garnet pyroxenites.

apparent inter-layering on different scales determined by modal variation of olivine and pyroxene (Fig. 2c). The layering is probably inherited from a primary igneous layering as seen in layered cumulates. The main constituent minerals are garnet, olivine, Opx, Cpx and minor Cr-rich spinel. Garnet pyroxenite is a minor component and occupies <2 vol.% of the peridotite massif. It occurs as (i) interlayers within garnet peridotite (Fig. 2d) and (ii) 2- to 5-m-thick dykes cross-cutting the layering of the massif (Song *et al.*, 2005a,b, 2007). The modal composition of garnet-pyroxenite is: garnet (20–30 vol.%), orthopyroxene (5–10%), clinopyroxene (40–60%) and phlogopite (2–5%). Olivine is absent. The documented associations and structures of the peridotite body in the field with its distinct and pronounced compositional layering suggests an Alaskan-type ultramafic cumulate complex origin and excludes an Abyssal peridotite protolith for the Luliangshan peridotite complex.

Bulk-rock composition data show that SiO_2 of the different peridotites range from 44.5 to 51.67 wt.%, MgO varies from 47.4 to 24.7 wt.% and Al_2O_3 ranges from 0.43 to 6.30 wt.%. The data show significant negative correlations of SiO_2-MgO, TiO_2-MgO, Al_2O_3-MgO and CaO-MgO except for garnet pyroxenite dykes and veins (Song *et al.*, 2007). The compositional trend is largely controlled by olivine-Opx fractionation.

The peridotites have varying contents of rare earth elements (REE) and other incompatible trace elements that increase with decreasing MgO as a result of varying olivine, Opx and Cpx modal variations. This suggests that these rocks are genetically related and that they have a cumulate origin. The chondrite-normalized REE patterns (Fig. 3) show that most garnet lherzolite samples have super-chondritic REE abundances, while all other peridotite samples have sub-chondritic REE abundances. All Luliangshan peridotites contain significantly higher REE concentrations than present-day abyssal peridotites and mantle wedge harzburgites (e.g. Niu, 2004; Song *et al.*, 2009c). The major element composition of garnet-free Luliangshan dunite suggests that it originally represents harzburgite from the sub-continental lithosphere. A conclusion that is also supported by model mineral compositions (see Song *et al.*, 2007). The rocks may have been metasomatically altered by melt also parental to the cumulate lithologies. All garnet pyroxenite and some garnet peridotite samples show similar *U*-shaped REE patterns with Light REE-enrichment with or without a negative Eu anomaly.

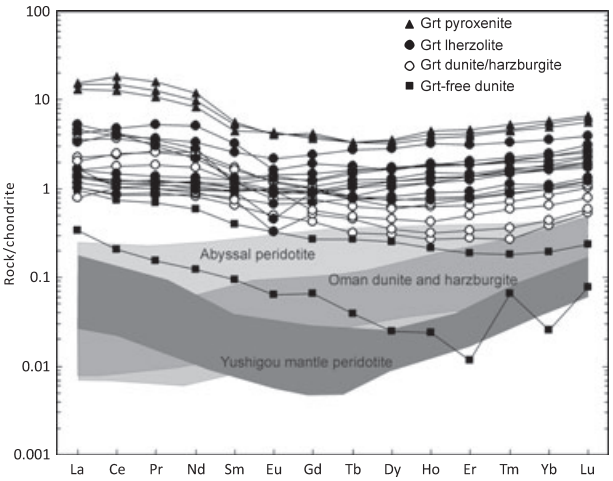

Fig. 3. Chondrite-normalized REE patterns for the Luliangshan garnet peridotite compared with present-day abyssal peridotite (Niu, 2004), Oman dunite and harzburgite (Godard *et al.*, 2000) and Yushigou mantle peridotite (Song *et al.*, 2009a,b).

Detailed mineral composition data have been reported by Song *et al.* (2007). Major rock-forming minerals, as controlled by whole-rock compositions, show large variations between rock types. Olivine from garnet-free dunite contains the highest X_{Mg} [Mg/(Mg + Fe)] ranging from 0.937 to 0.924 (sub-continental harzburgitic protolith; see above), olivine from garnet-bearing dunite/harzburgite has X_{Mg} from 0.920 to 0.906 and in garnet lherzolite X_{Mg} varies from 0.907 to 0.830. Such a wide range of olivine compositions (83–94 mol% Fo) is in considerable contrast with olivine compositions of the present-day abyssal peridotite, it rather resembles those of ultramafic cumulate complexes (Fig. 4a). As shown in Fig. 4b, average X_{Mg} of olivine is positively correlated with the whole-rock *mg*-number [$=$Mg/(Mg + Fe)] with a slope of $\sim$1. This suggests that X_{Mg} of olivine is controlled by the whole-rock composition during UHP and high temperature (HT) metamorphism. All orthopyroxene in Luliangshan garnet peridotites (including garnet lherzolite and garnet-bearing dunite) is extremely low in Al_2O_3 (0.3–0.9 wt.%). It also shows large X_{Mg} variations [Mg/(Mg + Fe)] from 0.94 to 0.96 in garnet-bearing dunite and from 0.87 to 0.93 in garnet lherzolite. The X_{Mg} of Opx correlates positively with the whole-rock *mg*-number (Fig. 4c) and also with X_{Mg} values of coexisting olivine.

Garnet crystals in the Luliangshan garnet peridotite are porphyroblasts of variable size (3–10 mm across). Almost all garnet exhibits kelyphitized rims consisting of Cpx, Opx and spinel that formed as a result of decompression. As expected, the pyrope component of garnet correlates positively whereas almandine correlates negatively with the whole-rock *mg*-number (Fig. 4d), suggesting that garnet is in equilibrium with coexisting minerals of the rocks.

Three porphyroblastic garnet crystals from garnet harzburgite and garnet lherzolite, respectively, have been analysed from core to rim by the Electron Probe Microanalyzer (EPMA). As shown in Fig. 5, these garnet crystals are rather homogeneous with no obvious compositional zoning; the major end-members in

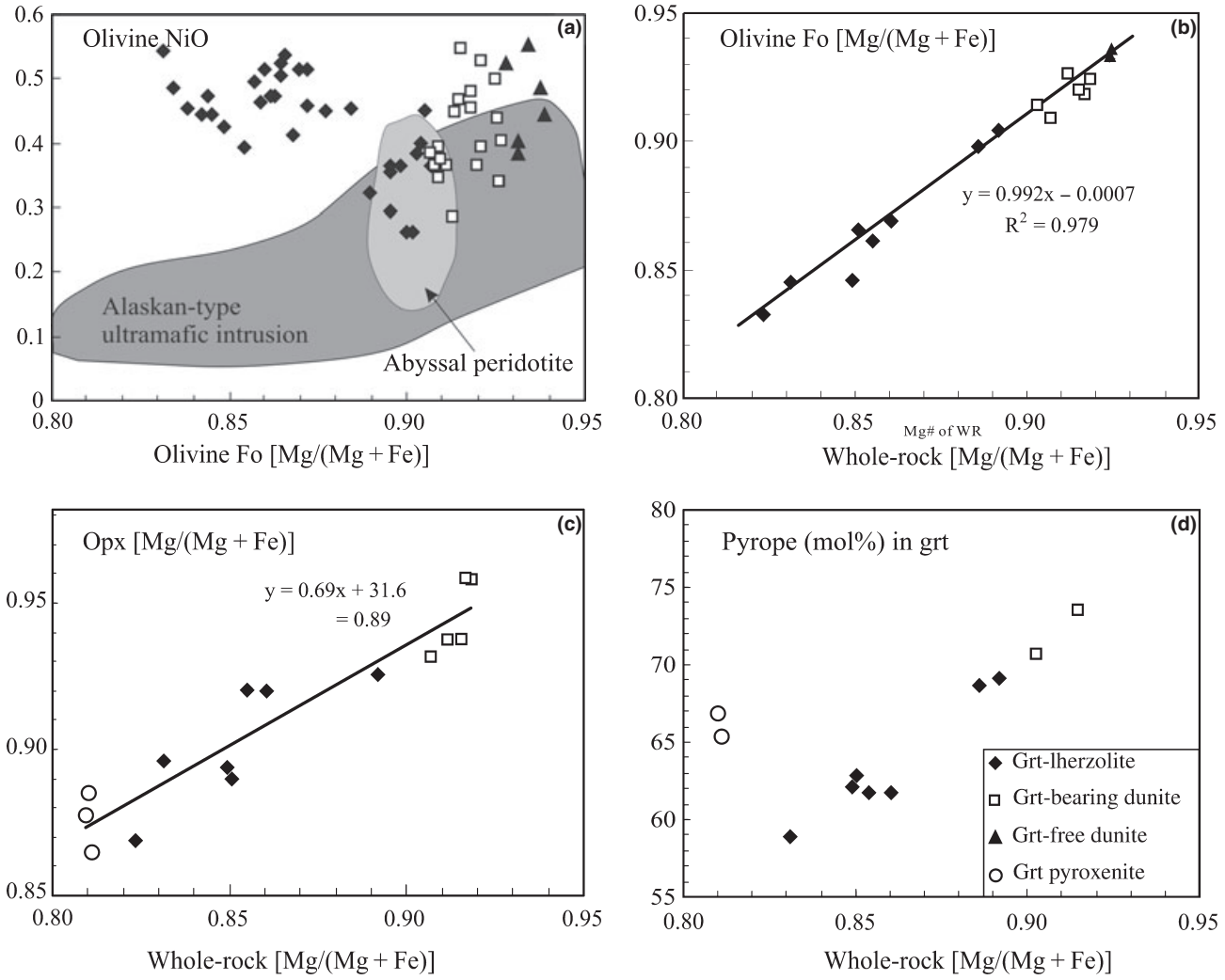

Fig. 4. (a) Fo (= [Mg/(Mg + Fe)]) *vs.* NiO content of olivine from the Luliangshan garnet peridotite compared with olivine from abyssal peridotite (Dick, 1989) and Alaskan-type ultramafic intrusion (Himmelberg & Loney, 1995; Batanova *et al.*, 2005). (b), (c) and (d) Whole-rock X_{Mg} [Mg/(Mg + Fe)] *vs.* [Mg/(Mg + Fe)] of olivine and Opx and pyrope content of garnet.

garnet crystals display flat patterns from core to rim. Sharp changes of pyrope and almandine proportions towards the rims are an effect of late kelyphitisation.

Clinopyroxene is generally diopside-rich in all rock types. Cr_2O_3 in Cpx from garnet lherzolite and garnet-bearing dunite varies from 0.6 to 1.6 wt%, whereas Cpx in garnet pyroxenite is Cr-poor (Cr_2O_3 = 0.18–0.30 wt%). X_{Mg} varies from 0.991 in the garnet-bearing dunite to 0.916 in the garnet lherzolite and correlate positively with X_{Mg} of olivine and orthopyroxene. The jadeite component of Cpx inclusions in garnet is higher (10.5–13.6 mol%) than in the matrix Cpx (0.7–9.6 mol%).

Amphibole (Amp) is a late phase in the rock matrix and grew at the expense of the high-grade mineral assemblage Grt + Opx + Cpx (+Ol) in all three rock types. Amphibole is mostly pargasitic in composition, occasionally cummingtonite was found.

METAMORPHIC EVOLUTION

Texture variation and *P–T* estimates

The four types of peridotite are coarse-grained undeformed rocks that have been altered to variable degrees by late deformation and serpentinization at shallow levels in the crust. The high-grade metamorphic assemblage of the garnet-free dunite is olivine + Cr-rich spinel ([Cr/(Cr + Al)] = 0.66–0.73) ± Opx. Olivine is strongly serpentinized and magnetite formed at serpentinized olivine grain boundaries. Equilibrium textures with straight grain boundaries and equilibrium three-grain contacts among the minerals of the pre-serpentinization assemblage are distinctive of HT metamorphism (Fig. 6a). Garnet is absent in dunite due to extremely low Al_2O_3 in the whole-rock composition. Garnet-bearing dunite/harzburgite with

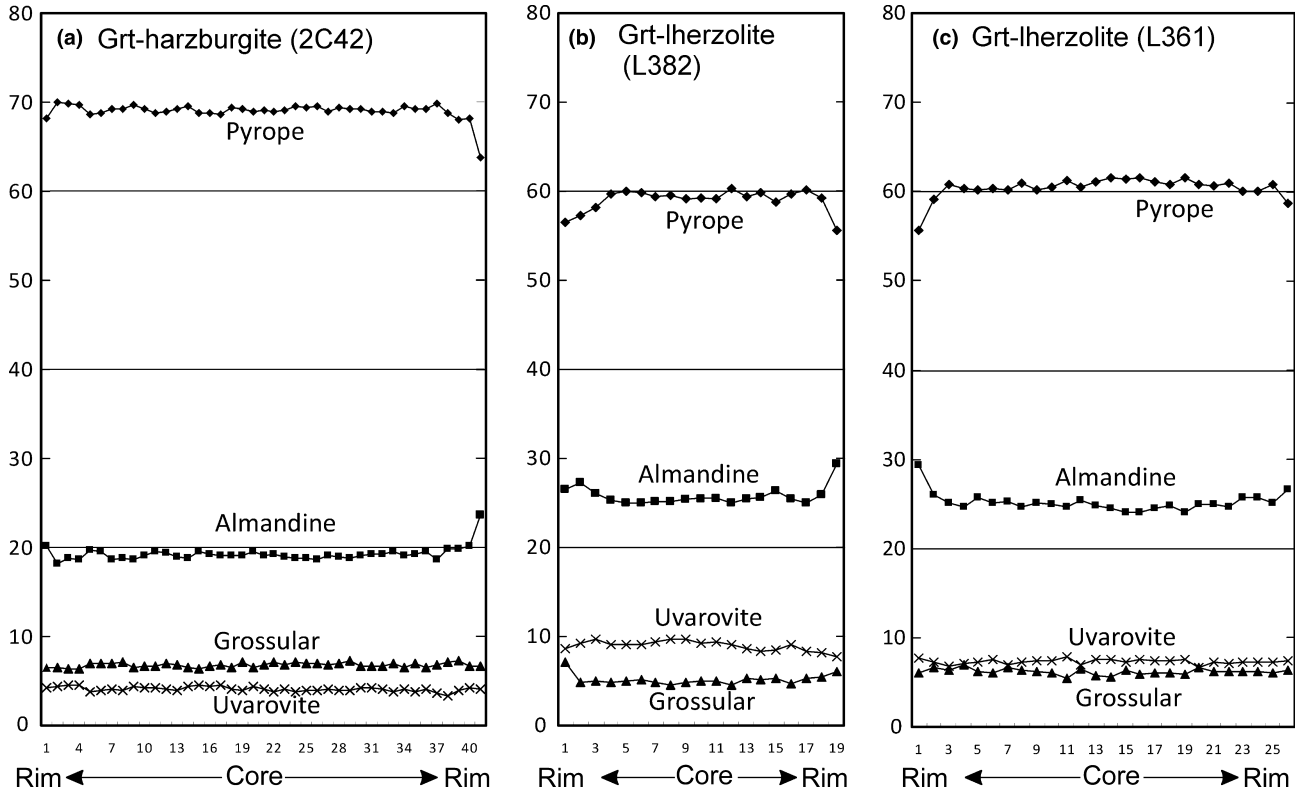

Fig. 5. Composition profiles of garnet from garnet harzburgite and lherzolite (mole%).

Grt + Ol + Opx ± Cpx shows similar coarse-grained equilibrium textures (Fig. 6b). Cr-spinel is probably a retrograde phase that may have formed from the breakdown of Cr-rich pyroxene and garnet (Fig. 6c). Much of the garnet lherzolite shows massive coarse-grained inequigranular to granoblastic textures. Some of the garnet lherzolite and garnet-olivine pyroxenite samples display primary cumulate textures with olivine occurring as inter-cumulus phase (Fig. 6d), in other samples Opx is inter-cumulus phase in olivine cumulates. The presence of cumulate texture indicates HT and low shear stress during its formation.

P–T estimates derived from various thermobarometers are listed in Table 1. Because all peridotites have experienced decompression, cooling and compositional re-equilibration during exhumation, estimated temperatures and pressures are minimum values. For garnet-bearing dunite, Al-in-Opx geobarometry (MacGregor, 1974; Nickel & Green, 1985; Brey & Koehler, 1990) yield metamorphic pressures of 4.6–5.3 GPa; Grt-Ol thermometry (O'Neill & Wood, 1979) gives temperatures of 980–1010 °C, and Ca-in-Opx thermometry (Brey & Koehler, 1990), 850–880 °C. Pressure estimates for garnet lherzolites range from 4.8 to 6.6 GPa, which overlap the calculated pressures for the garnet-bearing dunite. Temperature estimates by various methods in Table 1 range from 808–986 °C. The consistent *P–T* conditions (Table 1) derived from a variety of well calibrated geological thermometers and barometers are much higher than the 3.0–3.5 GPa and 700 °C calculated by Yang & Powell (2008) from dehydration equilibria of assumed hydrous minerals (see discussion below). The *P–T* estimates for garnet pyroxenite are lower than those for garnet peridotites, and the low *P–T* of 2C14 may represent the subsequent equilibrium during exhumation. However, the geothermobarometric data summarized in Table 1 imply that maximum *P–T* conditions of UHP metamorphism reached 4.6–6.6 GPa and 800–1000 °C. We consider 5.5 ± 1 GPa and 950 ± 50 °C for the peak conditions for plausible.

Zircon structure and mineral inclusions

Zircon is a mechanically stable accessory mineral and often preserves UHP inclusion phases (e.g. coesite and diamond) that it has captured during crystallization. The included UHP minerals are protected in refractory zircon from subsequent alteration and retrogression. Zircon also permits direct dating of the metamorphic history of country rocks as well as of garnet peridotite (e.g. Katayama *et al.*, 2001; Song *et al.*, 2006).

In general, zircon is rare in peridotites because of the very low level of Zr concentrations in mantle peridotite. The Luliangshan garnet peridotite, however, is unusually rich in zircon and some hundreds of zircon

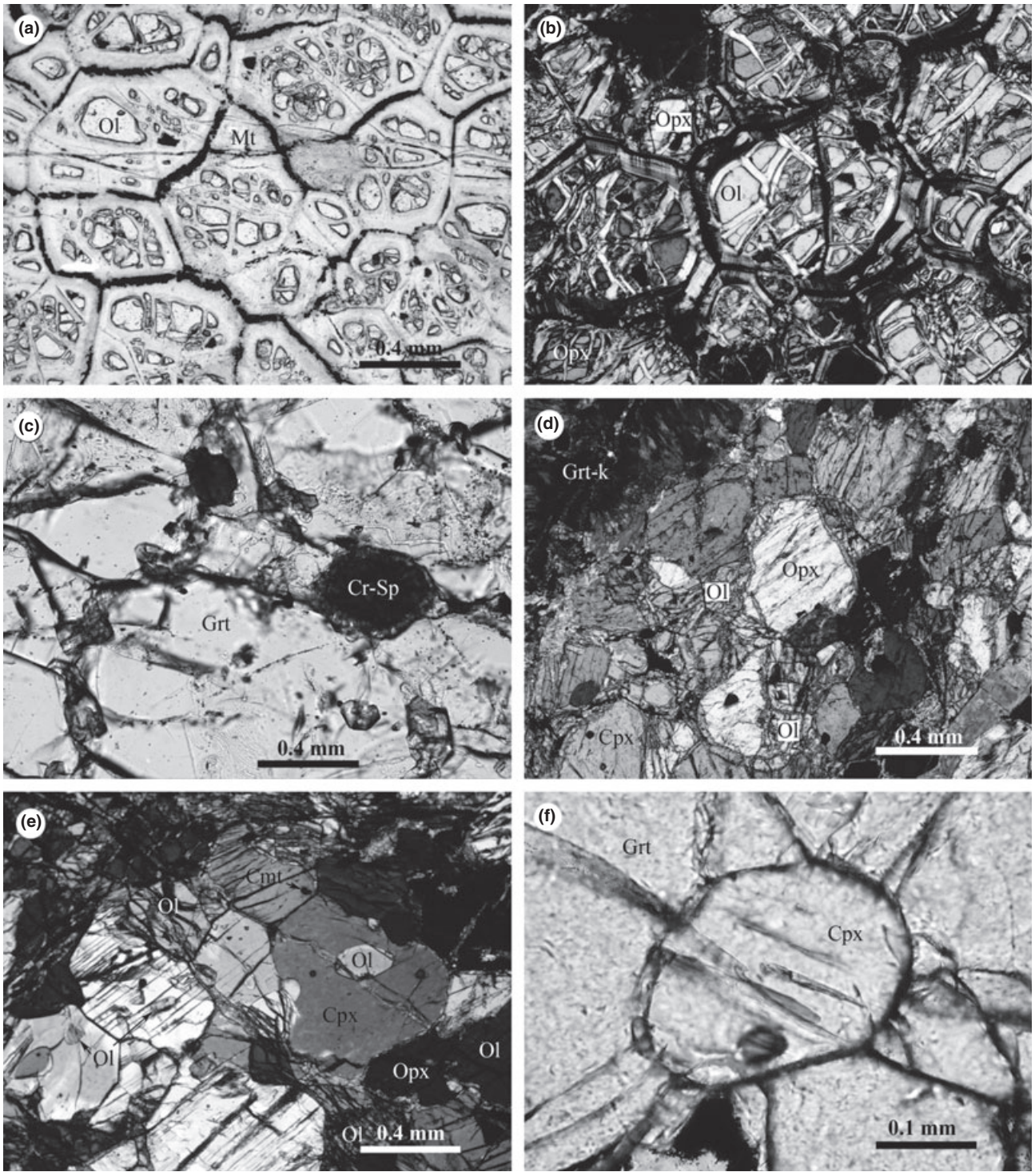

Fig. 6. Photomicrographs of the rock types from the Luliangshan garnet peridotite. (a) Serpentinized garnet-free dunite with fine-grained magnetite marking the boundaries of primary olivine grains. (b) Garnet-bearing dunite with pre-serpentinite equilibrium texture. (c) Retrograde Cr-rich spinel located along cracks in garnet. (d) Garnet lherzolite with cumulate texture showing inter-cumulus olivine. (e) Granoblastic texture of garnet lherzolite, olivine and Cr-magnetite occur as inclusions in pyroxene. (f) Radial fractures around Cpx inclusions in garnet from garnet lherzolite.

grains have been separated from garnet lherzolite (C305, 2C44), garnet-bearing dunite (2C39) and garnet pyroxenite (2C12, 2C78). The high modal zircon of the garnet-bearing ultramafic rocks strongly supports a magmatic/cumulate origin of the rock suite. Zircon crystals from garnet lherzolite are colourless,

Table 1. *P–T* data from the four rock types of the Luliangshan garnet peridotite.

Sample	2C13	2C14	2C36	2C39	2C41	2C42a	2C42b	2C44	2C50
Rock type	G-P	G-P	G-D	G-D	G-L	G-L	G-L	G-L	G-L
T opx-cpx [BK]	845	614			948	977	986	843	965
T opx-cpx [BM]	839	645			941	941	947	808	918
T opx-cpx [W]	868	727			923	923	937	862	939
T grt-ol [OW]			1012	984	812	828	847	965	843
T grt-opx [H]	1070	1073	992	987	908	851	851	918	920
T grt-cpx [EG]	811	814			847	847	855	827	860
T grt-cpx [P]	785	788			820	821	829	801	836
T Ca-in-opx [BK]	843	843	856	879	867	879	834	852	843
P grt-opx [BK]	3.96	2.61	5.23	4.64	4.87	6.57	6.56	5.18	5.04
P grt-opx [NG]	3.91	2.64	4.98	4.57	4.77	6.13	6.12	4.96	4.81
P grt-opx [MC]	4.27	2.89	5.26	4.71	4.87	5.37	5.37	4.99	4.99

Temperature (*T*) is in °C and pressure (*P*) is in GPa.
G-P, garnet pyroxenite; G-D, garnet-bearing dunite; G-L, garnet lherzolite; [BK], Brey & Koehler, 1990; [BM], Bertrand & Mercier, 1985; [W], Wells, 1977; [OW], O'Neill & Wood, 1979; [H], Harley, 1984; [EG], Ellis & Green, 1979; [P], Powell, 1985; [NG], Nickel & Green, 1985; [MC], MacGregor, 1974.

subhedral and show oval to elongated shapes from 50 to 250 μm in length. Most zircon crystals display clear internal zoning with cores and rims conspicuous microscopically under transmitted light. Combining zircon cathodoluminescent (CL) image analysis and SHRIMP dating, Song *et al.* (2005a,b, 2007) showed that the garnet lherzolite has experienced three events: (i) cores of most zircon crystals show characteristic oscillatory zoning and REE systematics (i.e. very high $[Lu/Sm]_{CN}$ = 88–230) suggesting a magmatic origin with crystallization ages of 484–444 Ma (weighted mean age, 457 ± 22 Ma). The data are consistent with a magmatic cumulate origin of the protoliths. The presence of olivine and Cpx inclusions in the zircon core domain (Fig. 7a,b) is also consistent with that zircon crystallized from a high-Mg magma; (ii) the mantle of the zircon containing inclusions of garnet, two pyroxenes, olivine and diamond (Song *et al.*, 2005a,b, 2007) gave ages of 435–414 Ma (with a mean of 423 ± 5 Ma), which represents the time of UHPM of the protoliths at depths of ~200 km; (iii) the rims of the zircon crystals yielded ages of 402–384 Ma (with a mean of 397 ± 6 Ma), which are thought to represent retrograde overprint during exhumation. The summarized zircon data indicate very deep subduction of continental cumulate material.

The size of roundish to oval shaped colourless zircon from the garnet-bearing dunite/harzburgite (2C39) is ~50–150 μm in diameter. Olivine and garnet (but no hydrous phase) inclusions are observed in some zircon by Raman spectroscopy and electron microprobe (Fig. 7c,d). Zircon from garnet pyroxenite (2C12 & 2C78) is colourless, roundish in shape and its morphology and internal structure is similar to that of zircon in the garnet-bearing dunite (Fig. 7e). Garnet, Cpx and Opx inclusions are present (Fig. 7f). CL images show that the internal structure of zircon from both garnet dunite and garnet pyroxenite is fairly homogeneous (Fig. 7d,f), suggesting that this zircon may have crystallized at HT (> > 700 °C) as seen in other high-grade (UHT) metamorphic rocks (e.g. Möller *et al.*, 2003; Hokada *et al.*, 2004).

Exsolution lamellae in rock-forming minerals

Most high-*P–T* minerals are complex solid solutions. They formed originally as compositionally uniform homogeneous single crystals at HT and HP. During decompression and cooling non-ideal solid solutions may become compositionally unstable. Hence, spinodal exsolution may separate an initially uniform single crystal *in situ* into physically and chemically distinctive crystals.

Exsolution lamellae are typical textures and products of phase separation resulting from decreasing *P–T*. The fine rods and bands of crystals exsolved from the mineral host in response to cooling (e.g. Cpx from Opx and vice versa) and decompression (e.g. Opx from garnet) (e.g. Dobrzhinetskaya *et al.*, 1996; Zhang & Liou, 1999, van Roermund & Drury, 1998; Song *et al.*, 2004). Cooling-induced exsolution such as perthite textures in feldspar and pyroxene unmixing is an ordinary phenomenon (e.g. Niu, 1997; Song *et al.*, 2009c). However, in recent years exsolution textures have been observed in UHP metamorphic rocks that clearly can be related to decompression (as a consequence of G_{ex} of mixing being a function of temperature and pressure). Reported decompression-related exsolution textures include: quartz/coesite lamellae from Cpx (Bakun-Czubarow, 1992; Tsai & Liou, 1998; Katayama *et al.*, 2000; Dobrzhinetskaya *et al.*, 2002; Song *et al.*, 2003a; Zhang *et al.*, 2005), coesite lamellae

Fig. 7. Zircon crystals and mineral inclusions from the Luliangshan garnet peridotite. (a) Olivine inclusion in magmatic zircon core from garnet lherzolite. (b) CL images showing magmatic cores and metamorphic mantle and rims. (c) Garnet, Opx and olivine inclusions in zircon crystals from garnet dunite. (d) CL images showing homogeneous structure of metamorphic zircon from garnet dunite. (e) Zircon crystals separated from garnet pyroxenite. (f) CL images showing homogeneous structure of metamorphic zircon from garnet pyroxenite with Opx and Cpx inclusions.

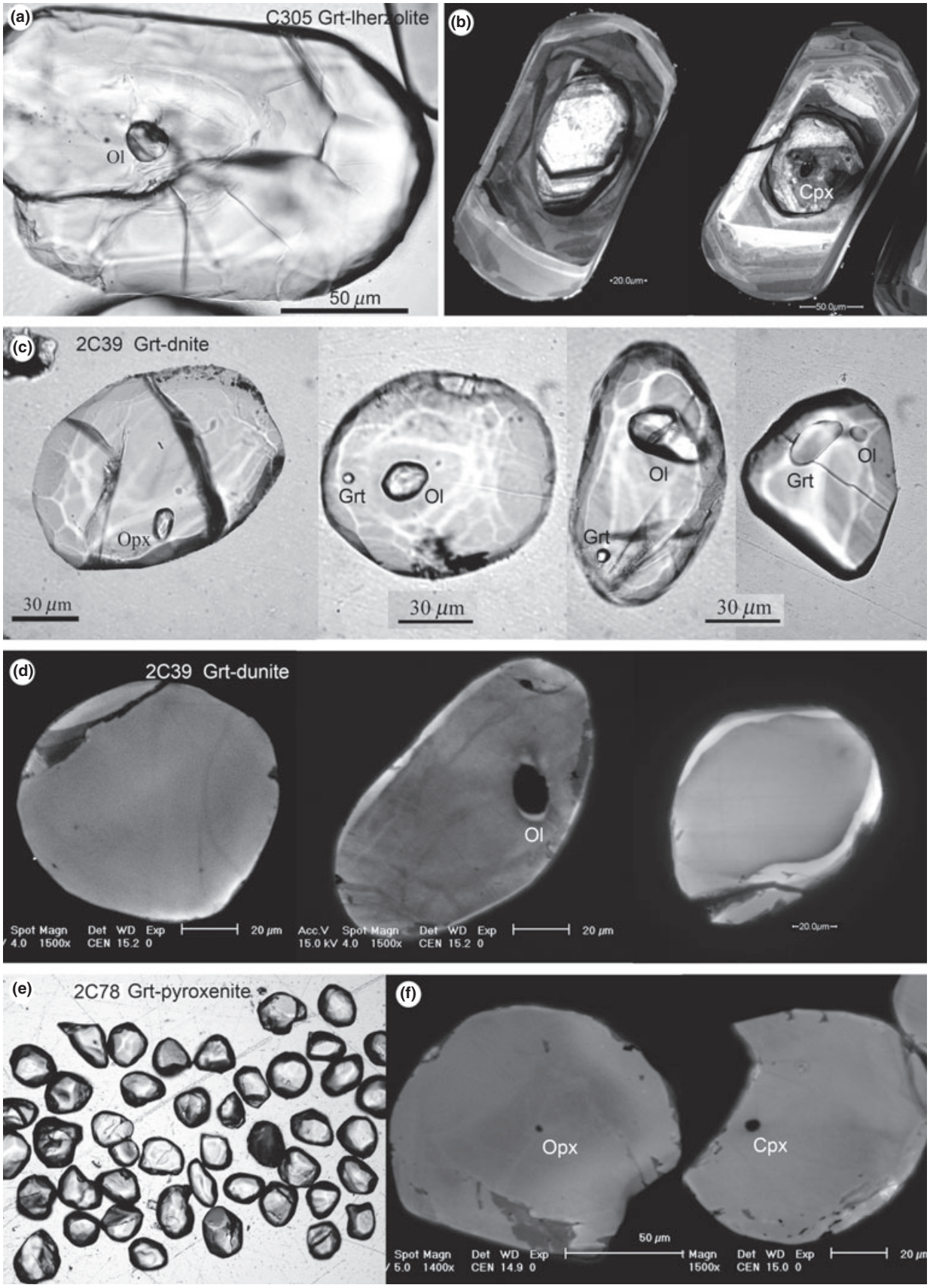

from supersilicic titanite (Ogasawara *et al.*, 2002), pyroxene lamellae from majoritic garnet (van Roermund & Drury 1998; Song *et al.*, 2004) and phlogopite lamellae from potassium-rich Cpx (Schmädicke & Müller, 2000; Zhu & Ogasawara, 2002; Bozhilov *et al.*, 2009). The important discovery of ilmenite exsolution rods in olivine from the Alpe Arami garnet peridotite (Dobrzhinetskaya *et al.*, 1996; Green *et al.*, 1997) marked a breakthrough in understanding continental deep (> 300 km) subduction and new geodynamic concepts (Hacker *et al.*, 1997; Pfiffner & Trommsdorff, 1998; Trommsdorff *et al.*, 2000; Risold *et al.*, 2001). The discovery of HP C2/c clinoenstatite (Bozhilov *et al.*, 1999) in the Alpe Arami garnet peridotite lends further support for the ultra-deep origin and exhumation from a depth in excess of 250 km of some garnet peridotites.

In the Luliangshan garnet peridotite, decompression-induced exsolution textures are very common in all peak metamorphic minerals including garnet, olivine and two pyroxenes in garnet-bearing dunite/harzburgite, garnet lherzolite and pyroxenite.

Exsolutions in olivine

Exsolutions in olivine from the Luliangshan garnet peridotite are rods or needles of ilmenite and chromium spinel (Song *et al.*, 2004). The ilmenite [(Fe, Mg)TiO_3] rods (~20–100 μm long and 0.3–3 μm wide/thick; Fig. 8a) are densely packed and well

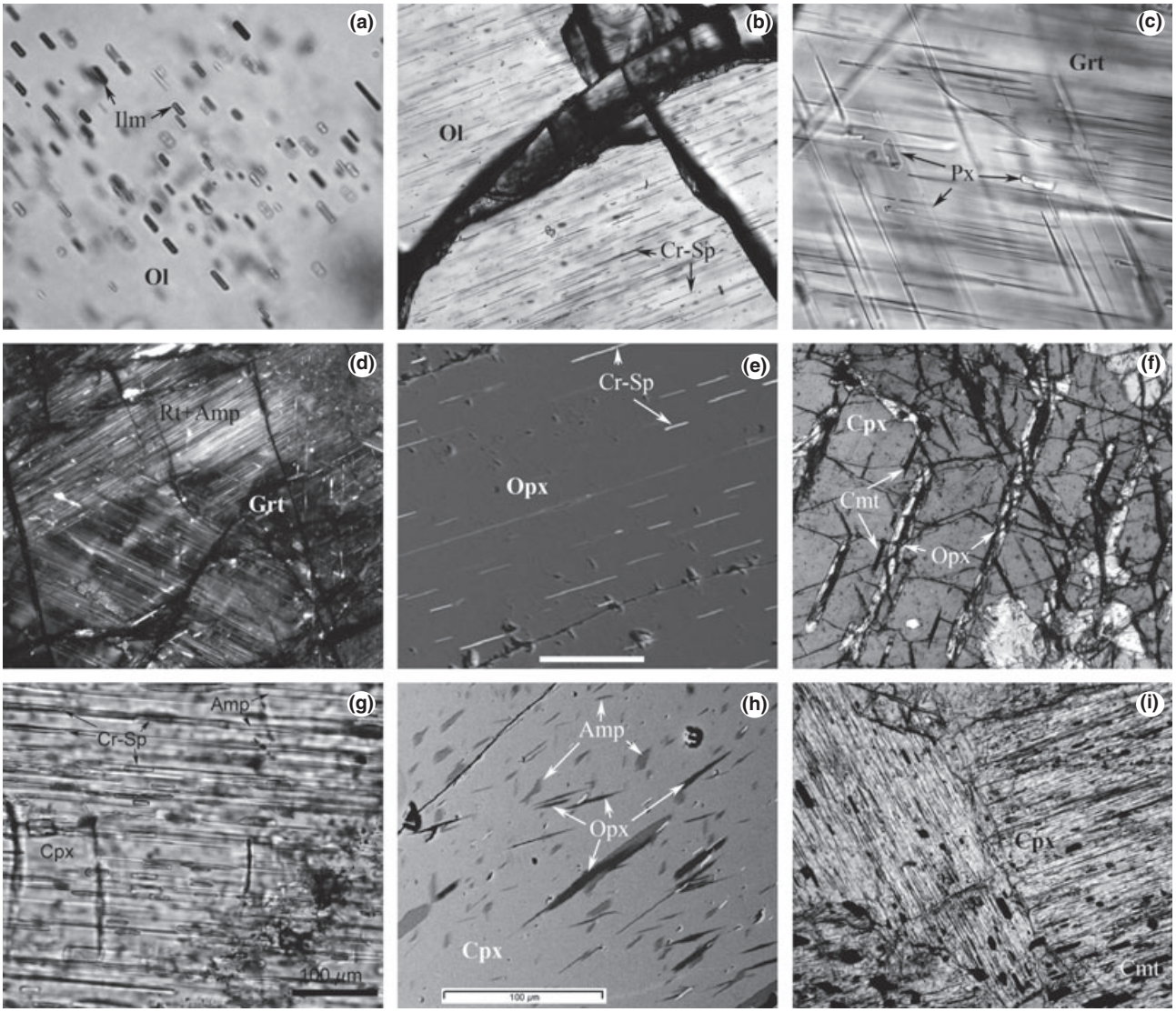

Fig. 8. Exsolution lamellae from major minerals from garnet peridotite and pyroxenite. (a) Ilmenite rods in olivine; (b) Cr-spinel needles in olivine; (c) pyroxene lamellae in garnet; (d) rutile + sodic amphibole lamellae in garnet; (e) Cr-spinel needles in opx (BSE image); (f) Opx and Cr-magnetite lamellae in Cpx; (g) Cr-spinel + Amp (+ quartz) lamellae in Cpx; (h) Opx + Amp lamellae in Cpx (BSE image); (i) Amp + quartz + Cr-magnetite lamellae in Cpx.

oriented, parallel to [010] of the olivine host. The abundance of the ilmenite rods corresponds to a maximum of ~0.7 wt.% ilmenite in olivine. The exsolution of ilmenite and Al-chromite needles (Fig. 8b) from the olivine is consistent with the peridotite once being equilibrated at very HP (> 300 km) (Dobrzhinetskaya *et al*., 1996). Experimental data also indicate that dissolution of such high TiO_2 content in olivine requires HT (> > 700 °C) (Dobrzhinetskaya *et al*., 1999).

Exsolution in garnet

Exsolution lamellae in garnet include densely packed rods of rutile, Opx, Cpx and sodic amphibole (Song *et al*., 2004, 2005a). The pyroxene exsolutions suggest that their parental garnet host crystals originally contained excess silicon (Fig. 8c), i.e. they were majoritic garnet that is only stable at depths well in excess of 150 km (Ringwood & Major, 1971; Irifune, 1987). Similar textures were also described in garnet from the Norwegian peridotite (van Roermund & Drury, 1998). The exsolution of rutile and sodic amphibole (Fig. 8d) further suggest that the inferred majoritic garnet also contains excess Ti, Na and hydroxyl that is only soluble at very HP of ≥7 GPa.

Exsolution in orthopyroxene

Decompression-induced exsolution needles are abundant in some porphyroblastic Opx (Fig. 8e). Energy-dispersive X-ray spectrometer scanning reveals that those needles are Cr-rich spinel, suggesting that the original host Opx was rich in Cr.

Exsolution in clinopyroxene

Clinopyroxene has complex exsolution products in various rock types. Exsolutions in Cpx from garnet dunite and lherzolite include three lamella assemblages: (i) Opx + Cr-magnetite (Cmt); (ii) amphibole + Cr-spinel and (iii) Opx + amphibole rods/lamellae (Fig. 9f–h). Exsolutions in Cpx from garnet pyroxenite mainly consist of densely packed lamellae of amphibole, quartz, Cr-magnetite (Fig. 8i) and minor phlogopite. These exsolutions are interpreted as resulting from decompression (Song *et al*., 2004, 2005a,b), which points to originally high-Si, Cr and hydroxyl in Cpx at peak metamorphic conditions. Back-scattered electronic images show that 8–10 vol.% amphibole lamellae and up to 4 vol.% quartz rods are present in some Cpx crystals. This means that the parental Cpx was supersilicic and also contained a significant amount of hydroxyl (~2000–3000 ppm). Similar observations have been reported in the UHP (> 6 GPa) Cpx of eclogites from the Kokchetav UHP terrane, Kazakhstan (Katayama & Nakajima, 2002) and of garnet peridotites from the Sulu terrane, eastern China (Chen & Xu, 2005).

Retrograde processes of the Luliangshan garnet peridotite

Most samples from the Luliangshan garnet peridotite massif have experienced various degrees of alteration/serpentinization during exhumation. On the basis of the detailed petrography, four stages of retrograde metamorphism can be recognized.

Stage I: solid exsolution

During the early stage of exhumation excess Si, Ti, Na, Cr and H in homogeneous UHP minerals separated into two or more phases in the host (e.g. pyroxene, rutile and sodic amphibole lamellae in garnet, ilmenite and Cr-spinel rods in olivine). The exact *P–T* conditions for the unmixing processes cannot be determined, but it is anticipated that they progressed within the stability field garnet + olivine (≥3.0 GPa; O'Hara *et al*., 1971).

Stage II: garnet kelyphitisation

Spinel-bearing symplectite around garnet (i.e. kelyphite) is a common feature of many garnet-peridotites. Kelyphite formation is related to decompression of garnet-peridotites from both UHPM terranes and kimberlite xenoliths (e.g. Godard & Martin, 2000). Kelyphite is an intergrowth texture of minerals, including two pyroxenes, spinel and occasionally amphibole (Fig. 9). It records the transition from UHP garnet peridotite to low-pressure (LP) spinel peridotite with continuous exhumation and decompression. At the garnet-spinel transition pyrope-rich garnet is replaced by Opx + Cpx + Spl at ≤3.0 GPa by the decomposition reaction:

$$[Mg, Fe, Ca]_3(Al, Cr)_2Si_3O_{12} \Rightarrow [Mg, Fe]_2Si_2O_6 + CaMgSi_2O_6 + [Mg, Fe](Al, Cr)_2O_4. \quad (1)$$

Released hydroxyl that has been dissolved in the UHP garnet forms a Amp + Spl symplectite. The kelyphitic structure, as shown in Fig. 9, occurs both as concentric coronas around and as pseudo-inclusion within relic garnet. Therefore, garnet kelyphitisation places an important constraint on the conditions of exhumation processes of UHP ultramafic rocks.

Stage III: amphibolite facies overprint

With exhumation to LP conditions, hydroxyl stored in the UHP Cpx and garnet (conceivably present as hydrogen at structural defects) can be released and may represent an important source of retrograde H_2O to form amphibolite facies assemblages (Zheng *et al*., 2003). This is substantiated by the presence of up to 6–8 vol.% amphibole exsolution lamellae in some Cpx crystals. At this stage, amphibole occurs either as large grains within the matrix replacing UHP minerals or around the outer rim of garnet kelyphite (Fig. 9a) or as small grains (pseudo-inclusions?) in garnet (Fig. 9e,f) and both pyroxenes.

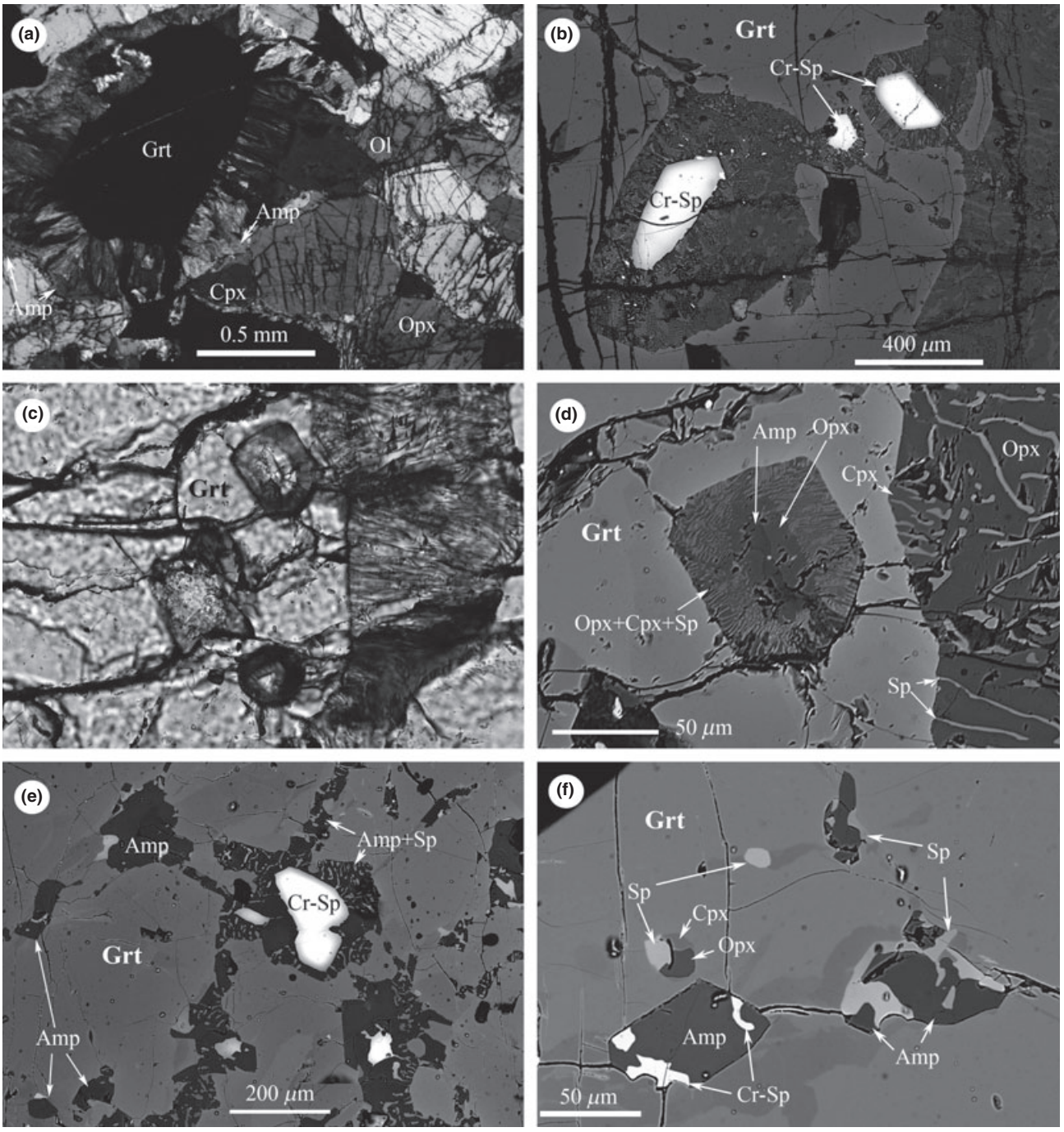

Fig. 9. Photomicrographs showing garnet retrogression textures from garnet peridotite. (a) Kelyphite texture around garnet, amphibole appears in the outer rim of the kelyphite. (b) Kelyphitisation both around and within garnet, Cr-rich spinel (Cr-Sp) occurs in the centre of Kelyphite texture (BSE image). (c) Kelyphitisation within garnet. (d) Enlarged BSE image of (c). (e) Amphibole + spinel kelyphite along cracks in garnet, the released Cr concentrated as Cr-rich spinel. (f) Amphibole within garnet formed by direct hydration of garnet (Amp 'inclusions' of Yang & Powell, 2008).

Stage IV: serpentinization

Serpentinization of peridotite is a fundamental rock-forming process that replaces olivine and pyroxene of peridotite by serpentine minerals and byproducts at LT and in H_2O-rich environments of the shallow crust. Figure 10(a) shows that the extent of serpentinization expressed by the loss-on-ignition (LOI; water dominated total volatiles) is proportional to bulk-rock MgO and modal olivine. However, serpentinization did not progress to completion and the peridotite assemblage is preserved in all rocks. In addition, serpentinization

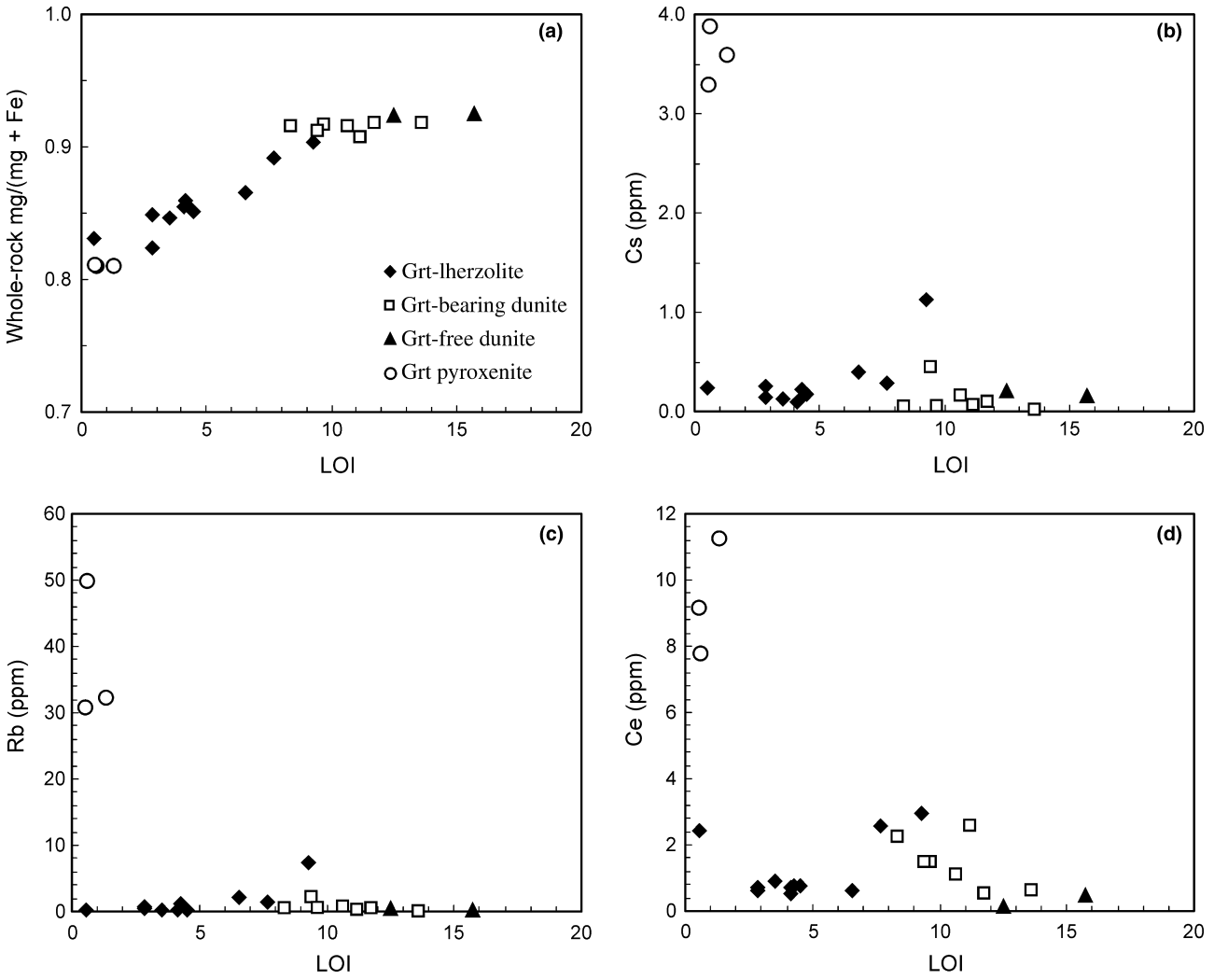

Fig. 10. Correlation of whole-rock water contents (LOI) with (a) X_{Mg} [MgO/(MgO + FeO)] and (b–d) trace elements soluble in aqueous fluids.

(in terms of LOI) did not change the amount of mobile elements (e.g. Cs, Rb, and LREE such as Ce) (Fig. 10b–d) suggesting that the buffer capacity of the peridotite has not been exhausted and serpentinization did not pervasively flush the peridotite. This partial internally controlled serpentinization is characteristic of peridotite hydration in continental crustal environments (Bucher-Nurminen, 1991).

DISCUSSION

The data and the analysis presented above confirm that the Luliangshan garnet peridotite massif experienced UHP (possibly >6.0 GPa) metamorphism and that the protolith derived from an ultramafic cumulate from primitive mantle melts in an mantle wedge environment most likely beneath an active continental margin (Song *et al.*, 2004, 2005b, 2007).

On the protolith of the Luliangshan garnet peridotite

It is important to note first that orogenic garnet peridotites are exclusively associated with UHP belts of continental-type subduction/collision, but they are absent in zones of oceanic lithosphere subduction. This observation points to a genetic association of garnet peridotite massifs with continental subduction and subsequent continental collision/exhumation.

Abyssal peridotites

Abyssal peridotites are mantle melting residues of middle-ocean ridge basalt (MORB) genesis produced beneath ocean ridges (e.g. Dick 1989; Niu 1997). Harzburgite is the dominant lithology with minor Cpx-poor lherzolite and dunite. They are mostly or entirely serpentinized as a result of seafloor hydrothermal

metamorphism in the vicinity of ocean ridges. In the context of global tectonic evolution, it is reasonable to infer that abyssal peridotites in the early Palaeozoic are petrologically and geochemically similar to the present-day abyssal peridotites. They are highly depleted with high-Mg and -Fe and very low Si, Ti, Al, Ca, Na and K (e.g. Niu, 2004). Olivine from abyssal peridotites have narrow X_{Mg} ranging from 0.89 to 0.91, rarely less than 0.88 or higher than 0.92 (e.g. Dick, 1989; Niu & Hékinian, 1997a,b). Because they represent melt residues depleted in basaltic component and oceanic peridotites often have low Al_2O_3 and lack garnet when metamorphosed under HP–UHP conditions. Good examples are metamorphosed harzburgites from the Shaliuhe ophiolite sequence, the Dulan terrane of this UHP belt (Zhang *et al*., 2008a; Song *et al*., 2009a,b), the Zermatt-Saas meta-harzburgites, Central Alps (Li *et al*., 2004) and the serpentinites in the North Qilian HP and LT belt (Song *et al*., 2009b).

Abyssal peridotites are typically strongly or completely serpentinized. Serpentinization transforms mantle olivine to Fe-poor serpentine minerals and oxidizes Fe of the fayalite component to magnetite. The later occurs in various textures including fine trails of dispersed magnetite along original olivine grain boundaries or between serpentine domains. Prograde metamorphism of serpentinites retains magnetite aggregate trails and prograde metamorphic olivine is typically extremely Mg-rich with X_{Mg} ranging from 0.94 to 0.99 (e.g. Bucher & Frey, 2002; Li *et al*., 2004; Zhang *et al*., 2008a,b; Song *et al*., 2009a,b). However, the documented low X_{Mg} of olivine from the Luliangshan garnet peridotite and the positive correlation between the olivine X_{Mg} and bulk-rock X_{Mg} (Fig. 5b) preclude an origin from serpentinized abyssal peridotite.

Further support for this conclusion comes from the depleted isotopic composition (e.g. $\epsilon_{Nd}(t) > 11$, 11.4–13.1; Wendt *et al*., 1997) of the abyssal peridotites, as MORB melt residues. The Luliangshan garnet peridotites are isotopically enriched (e.g. $\epsilon_{Nd}(t) < -0.5$, -6.8 to -0.5; Song *et al*., 2007), and must be associated with an enriched source (see below). Thus, serpentinized abyssal peridotites can be ruled out as protoliths of the Luliangshan garnet peridotite.

Mantle wedge peridotites

Mantle wedge peridotites are also highly depleted in major element compositions because of an even higher extent of partial melting than in abyssal peridotites (e.g. Arculus, 1994; Niu *et al*., 2003). As arc melting residues, they are anticipated to have more refractory olivine (Fo > 92) olivine spinel ($Cr^{\#} > 0.7$) (Dick *et al*., 1984; Arai *et al*., 2000). In this regard, the garnet-free dunite could be interpreted as mantle wedge melting residue, but this interpretation fails to explain garnet-bearing peridotites with evolved olivine having X_{Mg} as low as 0.83 (Fig. 4a)

Alaskan-type ultramafic cumulate lithologies

Ultramafic cumulate rock sequences resulting from crystallization of primitive mantle derived melts in a subduction-related environment have been labelled as 'Alaskan-type ultramafic intrusions' (e.g. Himmelberg & Loney, 1995). The intrusive assemblage consists of layered dunite, lherzolite and pyroxenite sequences with forsterite content of olivine varying from 94 to 80 mol.% (Batanova *et al*., 2005), analogous to the Luliangshan garnet peridotite.

The peridotites show compositional layering that is largely defined by modal variations of major minerals (garnet, olivine, orthopyroxene and clinopyroxene). Rhythmic crystallization bands of the protoliths can be convincingly inferred in some outcrops (Fig. 2c). These textural observations, together with relic accumulate textures in garnet lherzolite, the documented major and trace element systematics, as well as magmatic zircon cores, strongly suggest that the Luliangshan garnet peridotite ultramafic cumulate complex crystallized from high-Mg melts in an arc environment before UHP metamorphism. Normative igneous assemblages calculated from the bulk-rock major element compositions (Niu, 1997) vary from harzburgite to lherzolite, and to olivine websterite consistent with increasing bulk-rock Al_2O_3 (also modal garnet) and decreasing bulk-rock MgO (also modal olivine) during crystallization (see fig. 12 of Song *et al*., 2007).

The bulk-rock trace element systematics is consistent with the protoliths being in equilibrium with subduction-zone melts (see fig. 11 of Song *et al*., 2007) or being contaminated by continental crust material in their petrogenesis. Their enriched isotopic compositions (e.g. $\epsilon_{Nd}(t) < -0.5$, -6.8 to -0.5) and high enrichment in incompatible elements (Song *et al*., 2007) indeed suggest that a continental crust component has been incorporated in their parental melts either in the form of (subducted) terrigeneous sediments or from crustal contamination. Furthermore, the 700 Myr age of a zircon core (Song *et al*., 2005b) favours subduction-zone magmatism at an active continental margin. The accumulated and documented large volume of complementary data and observations is overwhelming evidence that the Luliangshan garnet peridotite originates from a late Precambrian Alaskan-type ultramafic intrusion.

Hydrous minerals in garnet and olivine of the Luliangshan garnet peridotite

Mineral inclusions in metamorphic porphyroblasts

Mineral inclusions particularly in porphyroblast host crystals are ubiquitous in metamorphic rocks. Mineral inclusions and the growth of porphyroblasts provide important information on the petrogenesis and metamorphic history (e.g. St-Onge, 1987; Spear, 1988, 1993; Liou *et al*., 1997; O'Brien, 1999).

Mineral species forming inclusions in porphyroblasts vary with *P–T* conditions and their sequence reflects the reaction history during porphyroblast growth. The inclusion minerals equilibrate with the host porphyroblast and represent frozen equilibrium states (Spear, 1993). Zircon in UHP rocks of the Kokchetav UHP terrane, in which inclusions change from the LP phases quartz, albite and graphite in the core domain, to the HP phase jadeite in the inner zone, and further to an UHP assemblage of jadeite, coesite and diamond in the mantle domain and, to a LP assemblage of quartz, plagioclase and graphite in the outer rim, revealing a *P–T* path from subduction to subsequent exhumation (Katayama *et al.*, 2001; Parkinson *et al.*, 2002). As a consequence, inclusions are snapshots of local equilibrium between inclusion and host porphyroblast, which, together with compositional changes from the core to rim of the porphyroblast, provide access to the *P–T* paths travelled by a metamorphic rock. However, it is important to distinguish mineral inclusions entrapped during porphyroblast growth and secondary minerals produced by reactions after entrapment in the porphyroblast during decompression and cooling.

Anhydrous mineral inclusions in garnet and pyroxene

In the Luliangshan garnet peridotite, mineral inclusions such as Cpx, olivine, Cr-magnetite (Cmt), occur in porphyroblastic garnet, pyroxene and olivine (Fig. 6e,f). These anhydrous inclusion species are identical to the peak mineral assemblage of the rock matrix.

Hydrous phases in garnet, olivine and pyroxene

Inclusions of hydrous minerals within the high-grade porphyroblasts are common in the strongly serpentinized Luliangshan peridotite. This includes composite amphibole + spinel inclusions in garnet, amphibole in pyroxene and serpentine and chlorite in olivine. Of course none of these hydrous phases have been entrapped during porphyroblast growth. Isolated serpentine inclusions in olivine of the Luliangshan peridotite have been described as lizardite (Yang & Powell, 2008), however, the reported composition suggests a mixture of lizardite and brucite probably being present.

In the matrix of the strongly serpentinized Luliangshan peridotite antigorite is the dominant serpentine mineral. This implies that serpentinization occurred via the stable reaction (Bucher & Frey, 2002; Frost & Beard, 2007):

$$\mathrm{Ol} + \mathrm{H_2O} + \mathrm{SiO_{2aq}} = \mathrm{Atg} + \mathrm{Mag} \qquad (2)$$

If SiO_{2aq} is provided by dissolution of Opx then stable serpentinization would occur at a pressure above ~2.2 GPa and temperature below 600 °C. If brucite is produced rather than SiO_{2aq} added, olivine is completely replaced by Atg + Brc + Mag at temperatures of ~400 °C in the presence of H_2O (Evans, 1977; Li *et al.*, 2004). This suggests that serpentinization of the Luliangshan peridotite complex started when the rocks cooled to ~600 °C and continued until supply of external water for the process ceased above 400 °C as the rocks were desiccated by the serpentinization process.

Lizardite (or chrysotile) may be produced by the metastable reaction forsterite + water = brucite + lizardite during very LT serpentinization (< 200 °C) (Wenner & Taylor, 1971; Evans, 1977, 2004; O'Hanley *et al.*, 1989). Upgrade, it breaks down via the stable reaction lizardite = antigorite + brucite at ~200 °C. Above this temperature lizardite cannot survive. It is important to note that prograde metamorphic olivine can and does exclusively grow in antigorite serpentinites. This is a consequence of serpentine mineral stability relationships and therefore prograde LT chrysotile or lizardite inclusions in olivine are impossible. Accordingly, lizardite in olivine represents a very LT metastable reaction product of a reaction probably caused by an aqueous fluid inclusion in olivine from earlier serpentinization to antigorite.

Both the texture and mineral assemblage of other hydrous mineral pseudo-inclusions in garnet are the same as those of the outer-rim kelyphite (Fig. 9), and are thus products of decompression exsolutions during exhumation. H_2O for the hydrous phases has probably been provided by unmixing H_2O originally dissolved in nominally 'anhydrous' UHP minerals.

CONCLUSIONS

The Qaidam garnet peridotite is a metamorphosed Alaskan-type ultramafic cumulate complex with dunite, harzburgite, lherzolite and pyroxenite. Abyssal peridotite can be excluded as protoliths of the garnet peridotites. Exsolution minerals and textures in high-*P–T* metamorphic minerals, including the presence of a diamond inclusion in a zircon, together with thermobarometric *P–T* calculations, suggest that the Luliangshan garnet peridotite has been subducted to depths of ~200 km and reaching temperatures in excess of 850–900 °C (possibly 950–1000 °C).

The Luliangshan garnet peridotite has experienced four stages of retrograde overprint during exhumation: (i) decompression-induced unmixing of the UHP minerals; (ii) garnet kelyphitisation; (iii) amphibole overprinting and (iv) serpentinization. Hydrous minerals occurring within peak metamorphic assemblage represent pseudo-inclusions, that is reaction products of reactions related to various stages of decompression and cooling rather than prograde inclusions during porphyroblast growth.

ACKNOWLEDGEMENTS

We contribute this study in honour of Harry W. Green for his tremendous contributions to Earth sciences.

This study was supported by Chinese National Natural Science Foundation grants no. 40825007, 40828002, 40773012, the Major State Basic Research Development Projects (2009CB825007) and the Foundation for the Author of National Excellent Doctoral Dissertation of PR China (200531). We thank two anonymous reviewers for their helpful review, and L. Dobrzhinetskaya and D. Robinson are appreciated for their constructive suggestions and editorial work on the manuscript.

REFERENCES

Arai, S., Hirai, H. & Uto, K., 2000. Mantle peridotite xenoliths from the Southwest Japan arc: a model for the sub-arc upper mantle structure and composition of the Western Pacific rim. *Journal of Mineralogical and Petrological Sciences*, **95,** 9–23.

Arculus, R.J., 1994. Aspects of magma genesis in arcs. *Lithos*, **33,** 189–208.

Bakun-Czubarow, N., 1992. Quartz pseudomorphs after coesite and quartz exsolutions in eclogitic omphacites of the Zlote Mountains in the Sudetes (SW Poland). *Archiwum Mineralogiczne*, **48,** 3–25.

Batanova, V.G., Pertsev, A.N., Kamenetsky, V.S., Ariskin, A.A., Mochalov, A.G. & Sobolev, A.V., 2005. Crustal evolution of Island-Arc Ultramafic Magma: galmoenan pyroxenite–dunite plutonic complex, Koryak Highland (Far East Russia). *Journal of Petrology*, **46,** 1345–1366.

Bertrand, P. & Mercier, J.-C. C., 1985. The mutual solubility of coexisting ortho- and clinopyroxene: toward an absolute geothermometer for the natural system? *Earth and Planetary Science Letters*, **76,** 109–122.

Bozhilov, K.N., Green, H.W. & Dobrzhinetskaya, L., 1999. Clinoenstatite in Alpe Arami peridotite: additional evidence of very high pressure. *Science*, **284,** 128–132.

Bozhilov, K.N., Xu, Z., Dobrzhinetskaya, L.F., Jin, Z.-M. & Green, H.W., 2009. Cation-deficient phlogopitic mica exsolution in diopside from garnet peridotite in Sulu, China. *Lithos*, **109,** 304–313.

Brey, G.P. & Koehler, T., 1990. Geothermobarometry in four-phase lherzolites II. New thermobarometers, and practical assessment of existing thermobarometers. *Journal of Petrology*, **31,** 1353–1378.

Bucher, K. & Frey, M., 2002. *Petrogenesis of Metamorphic Rocks*. Springer-Verlag, Berlin, Heidelberg, 341 pp.

Bucher-Nurminen, K., 1991. Mantle fragments in the Scandinavian Caledonides. *Tectonophysics*, **190,** 173–192.

Chen, J. & Xu, Z.Q., 2005. Pargasite and ilmenite exsolution texture in clinopyroxenes from the Hujialing garnet–pyroxenite, Su–Lu UHP terrane, Central China: a geodynamic implication. *European Journal of Mineralogy*, **17,** 895–903.

Chen, D.L., Liu, L., Sun, Y. & Liou, J.G., 2009. Geochemistry and zircon U–Pb dating and its implications of the Yukahe HP/UHP terrane, the North Qaidam, NW China. *Journal of Asian Earth Sciences*, **35,** 259–272.

Dick, H.J.B., 1989. Abyssal peridotites, very slowspreading ridges and ocean ridge magmatism. In: *Magmatism in the Ocean Basins*, *Special Publications 42*, (eds Saunders, A.D. & Norry, M.J.), pp. 71–105, Geological Society, London.

Dobrzhinetskaya, L., Green, H.W. & Wang, S., 1996. Alpe Arami: a peridotite massif from depths of more than 300 kilometers. *Science*, **271,** 1841–1845.

Dobrzhinetskaya, L., Bozhilov, K.N. & Green, H.W., 1999. The solubility of TiO_2 in olivine: implications for the mantle wedge environment. *Chemical Geology*, **160,** 357–370.

Dobrzhinetskaya, L.F., Schweinehage, R., Massonne, H.–. J. & Green, H.W., 2002. Silica precipitates in omphacite from eclogite at Alpe Arami, Switzerland: evidence of deep subduction. *Journal of Metamorphic Geology*, **20,** 481–492.

Ellis, D.J. & Green, D.H., 1979. An experimental study of the effect of Ca upon garnet-clinopyroxene Fe-Mg exchange equilibria. *Contributions to Mineralogy and Petrology*, **71,** 13–22.

Evans, B.W., 1977. Metamorphism of Alpine peridotite and serpentine. *Annual Reviews of Earth and Planetary Sciences*, **5,** 397–447.

Evans, B.W., 2004. The serpentinite multisystem revisited: chrysotile is metastable. *International Geology Review*, **46,** 479–506.

Frost, B.R. & Beard, J.S., 2007. On silica activity and serpentinization. *Journal of Petrology*, **48,** 1351–1368.

Godard, G. & Martin, S., 2000. Petrogenesis of kelyphites in garnet peridotites: a case study from the Ulten zone, Italian Alps. *Journal of Geodynamics*, **30,** 117–145.

Godard, M., Jousselin, D. & Bodinier, J.L., 2000. Relationships between geochemistry and structure beneath a palaeo-spreading centre: a study of the mantle section in the Oman ophiolite. *Earth and Planetary Science Letters*, **180,** 133–148.

Green, H.W., Dobrzhinetskaya, L., Riggs, E. & Jin, Z.-M., 1997. Alpe Arami: a peridotite massif from the mantle transition zone? *Tectonophysics*, **279,** 1–21.

Hacker, B., Sharp, T., Zhang, R.Y., Liou, J.G. & Hervig, R.L., 1997. Determining the origin of ultrahigh-pressure lherzolites (discussion). *Science*, **278,** 702–704.

Harley, S.L., 1984. An experimental study of the partitioning of Fe and Mg between garnet and orthopyroxene. *Contributions to Mineralogy and Petrology*, **86,** 359–373.

Himmelberg, G.R. & Loney, R.A., 1995. Characteristics and petrogenesis of Alaskan-type ultramafic–mafic intrusions, Southeastern Alaska. *US Geological Survey, Professional Papers*, **1564,** 1–47.

Hokada, T., Misawa, K., Yokoyama, K., Shiraishi, K. & Yamaguchi, A., 2004. SHRIMP and electron microprobe chronology of UHT metamorphism in the Napier Complex, East Antarctica: implications for zircon growth at $>1{,}000°C$. *Contributions to Mineralogy and Petrology*, **147,** 1–20.

Irifune, T., 1987. An experimental investigation of the pyroxene-garnet transformation in a pyrolite composition and its bearing on the constitution of the mantle. *Physics of the Earth and Planetary Interiors*, **45,** 324–336.

Katayama, I. & Nakajima, S., 2002. Hydroxyl in clinopyroxene from the deep subducted crust: evidence for H_2O transport into the mantle. *American Mineralogist*, **88,** 229–234.

Katayama, I., Parkinson, C.D., Okamoto, K., Nakajima, Y. & Maruyama, S., 2000. Supersilicic clinopyroxene and silica exsolution in UHPM eclogite and pelitic gneiss from the Kokchetav massif, Kazakhstan. *American Mineralogist*, **85,** 1368–1374.

Katayama, I., Maruyama, S., Parkinson, C.D., Terada, K. & Sano, Y., 2001. Ion micro-probe U–Pb zircon geochronology of peak and retrograde stages of ultrahigh-pressure metamorphic rocks from the Kokchetav massif, northern Kazakhstan. *Earth and Planetary Science Letters*, **188,** 185–198.

Li, X.-P., Rahn, M. & Bucher, K., 2004. Serpentinites of the Zermatt-Saas ophiolite complex and their texture evolution. *Journal of Metamorphic Geology*, **22,** 159–177.

Liou, J.G., Maruyama, S. & Ernst, W.G., 1997. Seeing a mountain in a grain of garnet. *Science*, **276,** 48–49.

MacGregor, I.D., 1974. The system MgO-Al_2O_3-SiO_2: solubility of Al_2O_3 in enstatite for spinel and garnet peridotite compositions. *American Mineralogist*, **59,** 110–119.

Mattinson, C.G., Wooden, J.L., Liou, J.G., Bird, D.K. & Wu, C.L., 2006. Age and duration of eclogite-facies metamorphism, North Qaidam HP/UHP terrane, western China. *American Journal of Science*, **306,** 683–711.

Mattinson, C.G., Wooden, J.L., Zhang, J. & Bird, D.K., 2009. Paragneiss zircon geochronology and trace element

geochemistry, North Qaidam HP/UHP terrane, western China. *Journal of Asian Earth Sciences*, **35,** 298–309.
Medaris, L.M. & Carswell, D.A., 1990. Petrogenesis of Mg-Cr garnet peridotites in European metamorphic belts. In: *Eclogite Facies Rocks* (ed. Carswell, D.A.), pp. 260–291. Blackie, Glasgow.
Möller, A., O'Brien, P.J., Kennedy, A. & Kröner, A., 2003. Linking growth episodes of zircon and metamorphic textures to zircon chemistry: an example from the ultrahigh-temperature granulites of Rogaland (SW Norway). In: *Geochronology: Linking the Isotopic Record with Petrology and Textures* (eds. Vance, D., Müller, W. & Villa, I.M.) *Special Publications 220*, pp. 65–81, Geological Society, London.
Nickel, K.G. & Green, D.H., 1985. Empirical geothermobarometry for garnet peridotites and implications for the nature of the lithosphere, kimberlites and diamonds. *Earth and Planetary Science Letters*, **73,** 158–170.
Niu, Y., 1997. Mantle melting and melt extraction processes beneath ocean ridges: evidence from abyssal peridotites. *Journal of Petrology*, **38,** 1047–1074.
Niu, Y., 2004. Bulk-rock major and trace element compositions of abyssal peridotites: implications for mantle melting, melt extraction and post-melting processes beneath mid-ocean ridges. *Journal of Petrology*, **45,** 2423–2458.
Niu, Y. & Hékinian, R., 1997a. Basaltic liquids and harzburgitic residues in the Garrett Transform: a case study at fast-spreading ridges. *Earth and Planetary Science Letters*, **146,** 243–258.
Niu, Y.L. & Hékinian, R., 1997b. Spreading-rate dependence of the extent of mantle melting beneath ocean ridges. *Nature*, **385,** 326–329.
Niu, Y.L., O'Hara, M.J. & Pearce, J.A., 2003. Initiation of subduction zones as a consequence of lateral compositional buoyancy contrast within the lithosphere: a petrologic perspective. *Journal of Petrology*, **44,** 851–866.
O'Hanley, D.S., Chernosky, J.V. & Wicks, F.J., 1989. The stability of lizardite and chrysotile. *Canadian Mineralogist*, **27,** 483–493.
O'Hara, M.J., Richardson, S.W. & Wilson, G., 1971. Garnet peridotite stability and occurrence in crust and mantle. *Contributions to Mineralogy and Petrology*, **32,** 48–68.
O'Neill, H. St. C. & Wood, B.J., 1979. An experimental study of Fe-Mg partitioning between carnet and olivine and its calibration as a geothermometer. *Contributions to Mineralogy and Petrology*, **70,** 59–70.
O'Brien, P.J., 1999. Asymmetric zoning profiles in garnet from HP-HT granulite and implications for volume and grain-boundary diffusion. *Mineralogical Magazine*, **63,** 227–238.
Ogasawara, Y., Fukasawa, K. & Maruyama, S., 2002. Coesite exsolution from supersilicic titanite in UHP marble from the Kokchetav Massif, northern Kazakhstan. *American Mineralogist*, **87,** 454–461.
Parkinson, C.D., Katayama, I., Liou, J.G. & Maruyama, S., 2002. *The Diamond-Bearing Kokchetav Massif, Kazakhstan: Petrochemistry and Tectonic Evolution of a Unique Ultrahigh-Pressure Metamorphic Terrane*. Universal Academy Press, Inc, Tokyo, 527 pp.
Pfiffner, M. & Trommsdorff, V., 1998. The high-pressure ultramafic-mafic-carbonate suite of Cima Lunga-Adula, Central Alps: excursions to Cima di Gagnone and Alpe Arami. *Schweizerische Mineralogische und Petrographische Mitteilungen*, **8,** 337–354.
Powell, R., 1985. Regression diagnostics and robust regression in geothermometer/geobarometer calibration: the garnet-clinopyroxene geothermometer revisited. *Journal of Metamorphic Geology*, **3,** 231–243.
Ringwood, A.E. & Major, A., 1971. Synthesis of majorite and other high pressure garnets and perovskites. *Earth and Planetary Science Letters*, **12,** 411–418.
Risold, A.-C., Trommsdorff, V. & Grobety, B., 2001. Genesis of ilmenite rods and palisades along humite-type defects in olivine from Alpe Arami. *Contributions to Mineralogy and Petrology*, **140,** 619–628.
van Roermund, H.L.M. & Drury, M.R., 1998. Ultra-high pressure (P > 6 GPa) garnet peridotites in Western Norway: exhumation of mantle rocks from >185 km depth. *Terra Nova*, **10,** 295–301.
van Roermund, H.L.M., Drury, M.R., Barnhoorn, A. & de Ronde, A., 2000. Super-silicic garnet microstructures from an orogenic garnet peridotite, evidence for an ultra-deep (>6 GPa) origin. *Journal of Metamorphic Geology*, **18,** 135–147.
van Roermund, H.L.M., Carswell, D.A., Drury, M.R. & Herjboer, T.C., 2002. Microdiamonds in a megacrystic garnet websterite pod from Bardane on the island of Fjørtoft, Western Norway: evidence for diamond formation in mantle rocks during deep continental subduction. *Geology*, **30,** 959–962.
Scheel, J.E., Nixon, G.T. & Scoates, J.S., 2005. New observations on the geology of the Turnagain Alaskan-Type Ultramafic intrusive suite and associated Ni-Cu-PGE mineralization, British Columbia. British Columbia Geological Survey, paper 2005-1, pp. 167–176.
Schmädicke, E. & Müller, W.F., 2000. Unusual exsolution phenomena in omphacite and partial replacement of phengite by phlogopite plus kyanite in an eclogite from the Erzgebirge. *Contributions to Mineralogy and Petrology*, **139,** 629–642.
Song, S.G., Yang, J.S., Xu, Z.Q., Liou, J.G., Wu, C.L. & Shi, R.D., 2003a. Metamorphic evolution of coesite-bearing UHP terrane in the North Qaidam, northern Tibet, NW China. *Journal of Metamorphic Geology*, **21,** 631–644.
Song, S.G., Yang, J.S., Liou, J.G., Wu, C.L., Shi, R.D. & Xu, Z.Q., 2003b. Petrology, geochemistry and isotopic ages of eclogites in the Dulan UHPM terrane, the North Qaidam, NW China. *Lithos*, **70,** 195–211.
Song, S.G., Zhang, L.F. & Niu, Y., 2004. Ultra-deep origin of garnet peridotite from the North Qaidam ultrahigh-pressure belt, Northern Tibetan Plateau, NW China. *American Mineralogist*, **89,** 1330–1336.
Song, S.G., Zhang, L.F., Chen, J., Liou, J.G. & Niu, Y., 2005a. Sodic amphibole exsolutions in garnet from garnet-peridotite, North Qaidam UHPM belt, NW China: implications for ultradeep-origin and hydroxyl defects in mantle garnets. *American Mineralogist*, **90,** 814–820.
Song, S.G., Zhang, L.F., Niu, Y.L., Su, L., Jian, P. & Liu, D.Y., 2005b. Geochronology of diamond-bearing zircons from garnet peridotite in the North Qaidam UHPM belt, Northern Tibetan Plateau: a record of complex histories from oceanic lithosphere subduction to continental collision. *Earth and Planetary Science Letters*, **234,** 99–118.
Song, S.G., Zhang, L.F., Niu, Y.L., Su, L., Song, B. & Liu, D.Y., 2006. Evolution from oceanic subduction to continental collision: a case study of the Northern Tibetan Plateau inferred from geochemical and geochronological data. *Journal of Petrology*, **47,** 435–455.
Song, S.G., Su, L., Niu, Y.L. & Zhang, L.F., 2007. Petrological and geochemical constraints on the origin of garnet peridotite in the North Qaidam ultrahigh-pressure Metamorphic Belt, Northwestern China. *Lithos*, **96,** 243–265.
Song, S.G., Niu, Y.L., Zhang, L.F., Wei, C.J., Liou, J.G. & Su, L., 2009a. Tectonic evolution of Early Paleozoic HP metamorphic rocks in the North Qilian Mountains, NW China: new perspectives. *Journal of Asian Earth Science*, **35,** 334–353.
Song, S.G., Su, L., Niu, Y., Zhang, G.B. & Zhang, L.F., 2009b. Two types of peridotite in North Qaidam UHPM belt and their tectonic implications for oceanic and continental subduction: a review. *Journal of Asian Earth Science*, **35,** 285–297.
Song, S.G., Su, L., Niu, Y., Lai, Y. & Zhang, L.F., 2009c. CH4 inclusions in orogenic harzburgite: evidence for reduced slab fluids and implication for redox melting in mantle wedge. *Geochimica et Cosmochimica Acta*, **73,** 1737–1754.
Spear, F.S., 1988. Metamorphic fractional crystallization and internal metamorphism by diffusional homogenization of

zoned garnets. *Contributions to Mineralogy and Petrology*, **99,** 507–517.
Spear, F.S., 1993. *Metamorphic Phase Equilibria and Pressure-Temperature-Time Paths*. Mineralogical Society of America, Washington, DC, 799 pp.
Spengler, D., van Roermund, H.L.M., Drury, M.R., Ottolini, L., Mason, P.R.D. & Davies, G.R., 2006. Deep origin and hot melting of an Archaean orogenic peridotite massif in Norway. *Nature*, **440,** 913–917.
St-Onge, M.R., 1987. Zoned Poikiloblastic Garnets: P–T Paths and Syn-Metamorphic Uplift through 30 km of Structural Depth, Wopmay Orogen, Canada. *Journal of Petrology*, **28,** 1–21.
Trommsdorff, V., Hermann, J., Müntener, O., Pfiffner, M. & Risold, A.-C., 2000. Geodynamic cycles of subcontinental lithosphere in the Central Alps and the Arami enigma. *Journal of Geodynamics*, **30,** 77–92.
Tsai, C.-O. & Liou, J.G., 1998. Eclogite-facies relics and inferred ultrahigh-pressure metamorphism in the North Dabie Complex, central-eastern China. *American Mineralogist*, **85,** 1–8.
Wan, Y.S., Xu, Z.Q., Yang, J.S. & Zhang, J.X., 2001. Ages and compositions of the Precambrian high-grade basement of the Qilian Terrane and its adjacent areas. *Acta Geologica Sinica*, **75,** 375–384.
Wells, P.R.A., 1977. Pyroxene thermometry in simple and complex systems. *Contributions to Mineralogy and Petrology*, **62,** 129–139.
Wendt, J.I., Regelous, M., Niu, Y.L., Hekinian, R. & Collerson, K.D., 1997. Geochemistry of lavas from the Garrett Transform Fault: insights into mantle heterogeneity beneath the eastern Pacific. *Earth and Planetary Science Letters*, **173,** 271–284.
Wenner, D.B. & Taylor, H.P., 1971. Temperatures of serpentinization of ultramafic rocks based on $0^{18}/0^{16}$ fractionation between coexisting serpentine and magnetite. *Contributions to Mineralogy and Petrology*, **32,** 165–185.
Yang, J.J. & Powell, R., 2008. Ultrahigh-pressure garnet peridotites from the devolatilization of sea-floor hydrated ultramafic rocks. *Journal of Metamorphic Geology*, **26,** 695–716.
Yang, J.J., Godard, G., Kienast, J.R., Lu, Y. & Sun, J., 1993. Ultrahigh-pressure (60 kbar) magnesite-bearing garnet peridotites from northeastern Jiangsu, China. *Journal of Geology*, **101,** 541–554.
Yang, J.J., Zhu, H., Deng, J.F., Zhou, T.Z. & Lai, S.C., 1994. Discovery of garnet-peridotite at the northern margin of the Qaidam Basin and its significance. *Acta Petrologica et Mineralogica*, **13,** 97–105 (in Chinese with English abstract).
Yang, J.S., Xu, Z.Q., Song, S.G. *et al*., 2001. Discovery of coesite in the North Qaidam Early Palaeozoic ultrahigh pressure (UHP) metamorphic belt, NW China. *Comptes Rendus De L Academie Des Sciences Serie II Fascicule A-Sciences De La Terre et Des Planetes*, **333,** 719–724.
Yang, J.S., Xu, Z.Q., Song, S.G. *et al*., 2002. Subduction of continental crust in the early Paleozoic North Qaidam ultrahigh-pressure metamorphism belt, NW China: evidence from the discovery of coesite in the belt. *Acta Geologica Sinica*, **76,** 63–68.
Zhang, R.Y. & Liou, J.G., 1999. Exsolution lamellae in minerals from ultrahigh-P rocks. *International Geology Review*, **41,** 981–993.
Zhang, R.Y., Liou, J.G. & Yang, J.S., 2000. Petrochemical constraints for dual origin of garnet peridotites of the Dabie-Sulu UHP terrane, China. *Journal of Metamorphic Geology*, **18,** 149–166.
Zhang, L.F., Song, S.G., AI, Y.L. & Liou, J.G., 2005. Relict coesite exsolution in omphacite from western Tianshan eclogites, China. *American Mineralogist*, **90,** 181–186.
Zhang, G.B., Song, S.G., Zhang, L.F. & Niu, Y.L., 2008a. The subducted oceanic crust within continental-type UHP metamorphic belt in the North Qaidam, NW China: evidence from petrology, geochemistry and geochronology. *Lithos*, **104,** 99–108.
Zhang, J.X., Mattinson, C.G., Meng, F., Wan, Y. & Dong, K., 2008b. Polyphase tectonothermal history recorded in granulitized gneisses from the North Qaidam HP/UHP metamorphic terrane, Western China: evidence from zircon U-Pb geochronology. *Geological Society of America Bulletin*, **120,** 732–749.
Zheng, Y.-F., Fu, B., Gong, B. & Li, L., 2003. Stable isotope geochemistry of ultrahigh pressure metamorphic rocks from the Dabie–Sulu orogen in China: implications for geodynamics and fluid regime. *Earth Science Review*, **62,** 105–161.
Zhu, Y.F. & Ogasawara, Y., 2002. Phlogopite and coesite exsolution from super-silicic clinopyroxene. *International Geology Review*, **44,** 831–836.

Received 3 March 2009; revision accepted 10 August 2009.